VOLUMETRIC DISPLAY BASED ON TWO-PHOTON ABSORPTION IN QUANTUM DOT DISPERSIONS

I. T. Lima, Jr, and V. R. Marinov
IEEE Journal of Display Technology, Vol. 6, No. 6, 2010, 221 – 228

Volumetric Display Based on Two-Photon Absorption in Quantum Dot Dispersions

Ivan T. Lima, Jr., *Senior Member, IEEE*, and Val R. Marinov

***Abstract*—A volumetric display technology based on two-photon absorption in quantum dots was investigated. We derive and validate a closed form expression for the luminance produced by dispersed quantum dots at the focal point of an infrared pulsed laser beam and we demonstrate using theory and experiments that voxels can be efficiently produced with commercially available solid-state pulsed lasers in off-the-shelf core-shell CdSe–ZnS quantum dots dispersed in toluene.**

***Index Terms*—Fluorescence, optical propagation in absorbing media, pulsed lasers, quantum dots (QDs), three-dimensional (3-D) displays.**

I. Introduction

THERE are numerous real-world applications involving vast amounts of data that must be comprehended by a user. If left unprocessed, the majority of this data is incomprehensible due to the limits of human processing. Visualizing information is one of the most efficient methods for accessing, processing, and understanding large data sets. Visualization is broadly defined as the process of communicating through visual information, by utilizing computer supported graphical representation of data that aids external cognition [1].

The world is three dimensional but the current display technology routinely visualizes it in two dimensions. Some of the three-dimensional (3-D) visualization technologies used in some specific applications today include holography, stereoscopic displays, and advanced 3-D graphics engines that generally render three dimensional images on a two dimensional display by mapping the coordinates of the 3-D images into a 2-D perspective. The use of these "pseudo" 3-D visualization technologies has a few drawbacks that result from the lack of true 3-D rendering. To view a three-dimensional visualization on a two-dimensional display such as a monitor screen, some method of projection must be used to render the three-dimensional geometry. As a result, some amount of geometric information is lost through this projection, reducing user's perception and, eventually, distorting the intention of the visualization [2]. Ultimately, these technologies lack the physiological depth cues needed for true 3-D display imaging such as motion parallax, accommodation, convergence, and binocular disparity [3].

Another class of 3-D displays includes the so-called *volumetric displays*. The difference between these displays and the 3-D designs discussed in the previous paragraph is that they form a visual representation of an object in three physical dimensions as opposed to the planar image of traditional screens. A comprehensive review on the various volumetric display designs that fall in this category is beyond the scope of this paper; interested readers are referred to the relevant literature [4]–[6].

The "true" volumetric displays project the image within a cube viewable from all or most of its sides and provide the ultimate physiological depth cues needed for a countless number of application including air traffic control, submarine undersea navigation, automotive design, architecture, and medical imaging, just to mention a few. This is the most "direct" form of a volumetric display in which an addressable volume of space is created out of active elements that are transparent in the *off* state but are either opaque or luminous in the *on* state. When these elements or *voxels* are activated, they show a solid pattern within the space of the display [7]. The display medium in most of the true 3-D displays disclosed in the literature is a solid material (a transparent polymer plastic, glass) with dispersed fluorescent particles such as crystals doped with rare earth ions [9]–[11], dye doped plastic [12], etc. Some displays use liquids, vapors, or fluorescent gases [3], [13]. Liquid- and vapor-based display media could be difficult to handle, operate, and, in some instances, are hazardous. Displays based on dyes suffer from low quantum efficiency and weak fluorescence. Furthermore, dyes degrade fairly quickly [14].

Another class of materials, the semiconductor nanocrystals or *quantum dots* (QDs), holds a promise of solving many of the problems with the traditional luminescence materials. QDs are an excellent material for displays because their quantum efficiency is very high, much higher than the quantum efficiency of other fluorescent materials such as fluorescent gas, dye, or doped crystals. Therefore, a high-luminance display can be designed using QDs without having to rely on high-power infrared laser radiation that is difficult to contain within the display volume and would be hazardous to the user and people nearby. The use of QDs uniformly dispersed in a transparent medium for volumetric displays has been vaguely described in the patent literature [15]. Unfortunately, the inventors have not provided any evidence and/or research results to support the feasibility of this idea.

The few true volumetric displays described in the relevant patent literature (none of these designs has been realized to

Manuscript received July 31, 2009; revised October 08, 2009. Current version published April 16, 2010.

I. T. Lima, Jr., is with the Department of Electrical and Computer Engineering, North Dakota State University, Fargo, ND 58108-6050 USA (e-mail: Ivan.Lima@ndsu.edu).

V. R. Marinov is with the Department of Industrial and Manufacturing Engineering, North Dakota State University, Fargo, ND 58108-6050 USA (e-mail: Valery.Marinov@ndsu.edu).

Color versions of one or more of the figures in this paper are available online at http://ieeexplore.ieee.org.

Digital Object Identifier 10.1109/JDT.2009.2037165

date) are built around the concept of two intersecting beams exciting the fluorescent material in the intersection between the two beams. However, as discussed later in this text, the optical properties of QDs are quite different from that of the fluorescent materials proposed for displays with two intersecting collimating beams. If one tries to exploit two-photon absorption in QD using two lasers with intersecting collimating beams and assuming that the sum of the energy of both photons matches the requirement for two-photon absorption in QD, the absorption will be very weak and the irradiance required will be much larger than the one needed to produce a voxel with the same luminance through two-photon absorption at the focal point of a single focused beam. The other problem with the two intersecting beams configuration is that the contrast between the interception point and the region illuminated by the two beams would be very small, just a factor of four that corresponds to a contrast ratio of only 6 dB, which is unacceptably low. Kimura *et al.* [16] reported the first 3-D single beam display that creates plasma dot arrays in the air at the focal point of the infrared pulsed laser at a rate of 100 dots per second. The dots are produced by supercontinuum generation in atmospheric air when the irradiance exceeds the multiphoton ionization threshold at the focal point of the laser, which is required to produce peak powers in excess of 3.2 GW [17]. This is four orders of magnitude higher than the power required in the technology explained later in this paper. This extremely high peak power poses a significant safety hazard and also substantially limits the pulse repetition rate of the laser. In addition, strong acoustic waves are produced at the focal point of the laser. Finally, it does not seem possible to create a color volumetric display using this approach.

II. Theoretical Basis of Display Technology

The two main components of any volumetric display are the display medium and the optical or electrical mechanism used to address and to turn on/off individual voxels. The display medium considered here consists of QDs dispersed in toluene. The dispersion medium was selected for its ease of use and for the sole purpose of demonstrating the theoretical principles of voxel generation in dispersed QDs. A real volumetric display based on these principles could use any other transparent host material—solid, liquid, or gaseous—provided that the dispersion medium does not adversely affect the optical properties of QDs or the overall operation and use of this device. The voxels are produced by exciting the QDs at the focal point of an invisible infrared beam that causes the QDs to emit light in the visible spectrum. The following subsections briefly discuss the display medium and the interaction of the laser light with the QDs.

A. Quantum Dots

The quantum dots are semiconductor nanocrystals of group II-VI (e.g. CdS, CdSe, CdTe, ZnS, ZnSe, ZnTe), or group III-V (e.g. GaAs, InAs, InGaAs, InP) capable of emitting electromagnetic radiation upon excitation. The wavelength of the emitted light depends on the size of the nanocrystal and the material. QDs have narrow emission bandwidth—from 20 to 40 nm—that scales with pump intensity. The larger the nanocrystal, the more red shifted and narrower the emission band is. QDs generally have a broad absorption band; the electromagnetic radiation absorption continuously increases from the onset, which occurs near to but at slightly higher energy than the emission peak. The unique optical properties of the QDs can be explained with the spatial quantum confinement effect. It is well known that the electronic and optical properties of materials are affected by size and shape. In the typical macroscale solid materials the bandgap (e.g., the interval between the top of the valence band and the bottom of the conduction band) remains at its original energy due to continuous allowed energy states outside the bandgap. In semiconductors, the Bohr exciton radius may be considerably larger than the lattice constant. In case of cadmium selenium, for example, the Bohr exciton radius is 4.9 nm [18] and the lattice constant of a zinc-blende (cubic) CdSe is 0.605 nm [19]. Modern technology provides opportunities for fabricating crystallite of semiconductor material with a size compatible with the Bohr exciton radius (for the example of CdSe that means a nanocrystal with several thousands of atoms on the average). In such low-dimension structures (named QDs by Mark A. Reed) the motion of the excitons in the crystallite will experience quantum confinement in all three directions. The effect of quantum confinement is that the allowed energy states are not continuous but quantized into a number of energy bands, forming a discrete spectrum that is controlled by the number of atoms, i.e., by the nanocrystal size.

While the quantum confinement has been studied experimentally and well understood theoretically [18], [20] the electron–phonon interaction in QDs remains a controversial subject [21]. The problem is complicated by the fact that in real structures containing QDs, the latter are embedded in a dielectric medium with a dielectric constant typically smaller than the dielectric constant of the QD. For example, organic molecules could be used to "cap" the outer surface of core semiconductor nanocrystals to prevent the aggregation and oxidation or the core could be enclosed in a shell of another semiconductor. The difference in the dielectric constants gives rise to surface polarization effects [22], [23]. Moreover, the interface between the QD and surrounding material cannot be considered as an infinite potential barrier and the simple *particle-in-a-box* theoretical analysis in which the confinement space has an infinite potential at its boundaries is not directly applicable. Both effects together may result in instabilities such as self-trapping of carriers at the QD surface [24]. In this case, the electron-hole pair state evolves from a volume state in which the pair is inside the QD, to a surface-trapped state in which the radial charge distribution is concentrated near the surface [18]. This transition modifies substantially the emission properties of the embedded QDs. For example, the core-shell type QDs, such as the ones with optical characteristics described in Table I, exhibit different optical properties than the core material [25].

QDs are an excellent material for displays because of the following properties [18]: 1) their quantum efficiency is very high, much higher than the quantum efficiency of other fluorescent materials such as fluorescent gas, dye, or doped crystals. Therefore, a high-luminance display can be designed without having to rely on high-power infrared laser radiation; 2) color tunability of the luminescence is easily obtained through size

TABLE I
OPTICAL PROPERTIES OF 560 nm CdSe/ZnS QDs

Parameter	Value
Emission peak, λ_e:	560 nm
Quantum efficiency, Φ:	0.4
Absorption peak (1st exciton), λ_a:	545 nm
Extinct. coeff. 1st exciton peak, ε:	0.98×10^5 L·mol^{-1}·cm^{-1}
Abs. coeff. 1st exciton peak, σ_a:	2.25×10^5 L·mol^{-1}·cm^{-1}
TPA coefficient at 2× wavelength of 1st exciton peak, Σ:	10^4 GM, where 1 GM = 10^{-50} cm^4·s·photon^{-1}

control; 3) the luminescence of QDs is very narrow, i.e., spectrally pure (although Bowers and co-workers have recently reported a white-light emission from so-called "magic-size" QD [27]); 4) the QDs are photostable; and 5) the absorption lineshape of the QDs continues above an onset (which depends on particle size). Therefore, the luminescent QDs are capable of being excited over a broad bandwidth, yet exhibit emission in a narrow wavelength band. For the monochromatic display described here, one possible fluorescence material would be the QDs in Table I. Their 560-nm emission peak is close to the peak sensitivity of the human eye in photoptic vision (555 nm). It can be shown that QDs with different emission bands can be used to produce a volumetric color display but this discussion is beyond the scope of this paper.

B. Upconversion Photoluminescence in QDs

The fundamental process in the described display is the upconversion photoluminescence initiated in the QDs by a focused infrared laser beam. The upconverted or anti-Stokes photoluminescence (UCPL) is the emission of photons with energies higher than the excitation energy. The UCPL occurs when the QDs are excited with light sources operating at wavelengths much longer (i.e., lower energy photons) than the ones in the absorption spectrum that produces the normal photoluminescence (PL) band.

Several studies on QDs, including CdTe, InP, and CdSe QDs [29]–[32], have found that the UCPL increases linearly with the excitation power that, according to the interpretations offered by the authors, means that processes like *two-photon absorption* (TPA) and, since the possibility of emergence of more than one exciton per QD is negligible, Auger excitation can be excluded. Based on these observations, the authors of these studies concluded that in their experiments the UCPL mechanism would involve a single-photon excitation through intermediate sub-gap states to the higher energy (luminescent) states. On the contrary, other researchers investigating the same type of QDs (CdTe and CdSe) and other types such as CdS, have reported a quadratic or nearly quadratic dependence between the emittance and excitation power, which is a strong indicator of a TPA process [33]–[38]. Thantu [39] carried out time-resolved experiments to show that a significant part of the UCPL produced by a borosilicate glass doped with ZnSe QDs results from second-harmonic generation (SHG). Jacobsohn and Banin [39] studied size dependence of the SHG in CdSe QDs dispersed in toluene. They reported that the observed SHG emission was a several orders of magnitude weaker than that caused by a TPA. SHG is easily differentiated from TPA because there is no absorption process in SHG. Therefore, the response time in SHG is much faster than the luminescence that is produced after TPA in a fluorescent material. If SHG was also efficient in QDs embedded in other transparent hosts, the visible UCPL from those QDs could be tuned by the appropriate choice of the pump wavelength. However, since SHG is a coherent effect, it is generated along the same direction as the excitation source. Therefore, the SHG is not as effective as the TPA in producing voxels in volumetric displays.

The differences in the UCPL mechanisms suggested in the literature are likely due to the differences in the QDs structure and different materials used in the nanocrystal core and, when present, in the nanocrystal shell, the presence of surface defects on the core and shell surfaces, and the properties of the host material in which the QDs were dispersed. Most of these parameters are dependent on the process used to synthesize the nanocrystals. The QDs with linear dependence of the UCPL can be used as fluorescence targets due to their efficient excitation, while the QDs with quadratic dependence of the UCPL can be efficiently used for confocal imaging [33] and, if the UCPL is primarily due to TPA, for voxel generation in volumetric displays resulting from selective excitation near the focal point of the laser beam.

The absorption cross-section of the QDs is much higher that this of the traditional fluorescent materials. Pu *et al.* [38] have investigated the size-dependent TPA cross section of II-VI QDs and have found that the TPA cross section is empirically related via a power-law proportionality of 3.5 ± 0.5 and 5.6 ± 0.7 to the diameters of CdSe and CdTe QDs. They attributed their results to the intrinsic TPA properties of the QDs. Chon *et al.* [41] reported a three-photon excitation of CdS QDs exciting the nanocrystals with a Ti:sapphire femtosecond laser operating at a pulse width of 100 fs, a repetition rate of 80 MHz, and a wavelength range from 900 nm to 1000 nm. The authors measured the TPA cross section of CdSe QDs to be approximately $\sim 10^{-46}$ cm^4 s photon^{-1}, which is two to three orders of magnitude higher than the value for the common fluorescent dyes. The three-photon absorption cross section of the same material was also measured and found to be $\sim 10^{-79}$ cm^6 s^2 photon^{-2}, or three to four orders of magnitude higher than those of the previously reported common fluorescent dyes. These results once again illustrate how efficient QDs can be as a display material in volumetric displays.

It is obvious from the reported results that the simplified analyses based on the elementary quantum mechanics alone may not be sufficient to explain some of specifics of the UCPL in systems with practical applications such as QDs embedded in dielectric materials and often times enclosed in a thin shell of a second semiconductor with larger band gap (e.g., ZnS capped CdSe QDs), or passivated with a monolayer of TOPO (tri-n-octyl phosphene oxide) molecules to eliminate electron surface traps. The intrinsic properties of the host medium and the surface effects in the QDs need all to be taken into account.

It is hypothesized that some of the observed phenomena in the UCPL of embedded QDs, such as the redshift in the emitted light, are due to the presence of these surface states [29], [31], [33], [42]. The importance of studying the entire system, not only the QDs, is illustrated by the fact that in solids the UCPL spectrum is significantly redshifted relative to the PL spectrum, whereas in solutions using the same QDs there is a very little spectral shift [37].

The conclusion from the above discussion is that the UCPL due to TPA is presumably the most efficient mechanism for generating voxels in QDs embedded in a transparent host medium and, ultimately, for building a volumetric display. For that reason the focus in our study is on the embedded capped QDs in which the UCPL has quadratic dependence on the excitation irradiance. In these nanocrystals, the TPA is the main mechanisms for UCPL at room temperature. A characteristic of the upconversion emission from QDs through TPA is the quadratic or near-quadratic laser power dependence, $I \sim P^{\mathrm{K}}$, where I is the emitance, P is the instantaneous power of the pump source, and K is an exponent with values between 2.0 and 1.7 that depends on the size (color) of the QDs [33]. Therefore, the luminance of a voxel in the volumetric display could be considered directly proportional to the square of the laser pump power and inversely proportional to a higher power on the diameter of the excited region [10]. In the next section we derive theoretically a relationship for the dependence of the voxel luminance on the pump irradiance and voxel diameter using the physics of TPA and beam optics. The results indicate that we can control the luminance of a given voxel by modulating the pump laser power.

C. Theory of Voxel Generation in QDs

One of the questions addressed in this study is what optimal concentration of QDs in the display medium is required to generate voxels with sufficient emittance. A too large QD concentration will attenuate the light emitted by the voxels before it crosses the boundaries of the volumetric display as a result of the one-photon absorption because of the strong overlap between the QDs absorption and the emission spectra. A too small QD concentration would not provide sufficient luminance. There is obviously a range of operational values for the QD concentration that needs to be experimentally determined. It is logical to assume that the optimal value of the QD concentration will be close to the lower end of this range. This will ensure sufficient brightness from the voxel without saturating the display medium with too much active material. In this section we derive an expression for the luminance of the voxels at 555 nm (green), which is the wavelength at which the photoptic human vision is the most sensitive. This expression can be easily extended to other wavelengths, including red and blue, for which the photoptic human vision is less sensitive.

A typical laptop monitor has a luminance between 100 nit and 250 nit ($1\ \mathrm{nit} = 1\ \mathrm{cd} \cdot \mathrm{m}^{-2}$) [43]. The irradiance, I, in case of unsaturated TPA is given by [44]

$$dI/dz = -\beta I^2 \tag{1}$$

where $\beta = 2C\Sigma/(h\nu)$ and C is the concentration. Therefore, the TPA cross-section $\sigma_{2\mathrm{p}}$ at the first exciton is given by

$$\sigma_{2p} = \frac{\beta}{C} = \frac{2\Sigma}{h\nu} = 6.95 \times 10^{-36}\ \mathrm{m}^4 \cdot \mathrm{s} \cdot \mathrm{J}^{-1}. \tag{2}$$

The solution to (1) is given by

$$I(z) = \frac{I_0}{1 + \beta I_0 z} = \frac{I_0}{1 + \sigma_{2p} C I_0 z}. \tag{3}$$

If the medium is unsaturated and highly transparent, the irradiance variation, ΔI, due to the absorption along the propagation direction z is given by

$$\Delta I(z) \cong \sigma_{2p} C I_0^2 z. \tag{4}$$

This corresponds to the regime in which we expect the volumetric display to operate.

The voxel dimension produced by TPA is defined by the spatial dependence of the irradiance squared, I^2. We define the voxel dimensions as the lengths in which I^2 decreases by half when compared with the peak irradiance squared, I_0^2. These dimensions are essentially the full-width at half-maximum (FWHM) of I^2.

Following Saleh and Teich [45], the irradiance I and the beam radius W of a Gaussian beam (TEM_{00}) can be expressed as a function of the transversal ρ and the longitudinal z coordinate as follows:

$$I(\rho, z) = \frac{2P}{\pi W^2(z)} \exp\left[\frac{-2p}{W^2(z)}\right] \tag{5}$$

and

$$W(z) = W_0 \left[1 + \left(\frac{z}{z_0}\right)^2\right]^{1/2} \tag{6}$$

where P is the optical power, I_{o} is the irradiance, W_{o} is the beam waist radius, and z_{o} is the Rayleigh range of beam. The Rayleigh range of a Gaussian beam is the distance from the beam waist in which the beam diameter increases by a factor $2^{1/2}$, which can be calculated from (5) and (6)

$$z_0 = \frac{\pi W_0^2}{\lambda}. \tag{7}$$

Then, the voxel radius, W_{vx}, and the longitudinal length of the voxel, L_{vx}, are given by

$$W_{vx} = \frac{\sqrt{\ln(2)}}{2} W_0' \quad \text{and} \quad \mathrm{L}_{vx} = 2z_0'. \tag{8}$$

The prime parameters W_0' and z_0' in (8) indicate the beam waist radius and Rayleigh range, respectively, after the laser beam is focused by a lens to form a voxel. If the lens is located at the waist of the laser beam, the focused beam waist and Rayleigh range are given by [45]

$$W_0' = \frac{W_0}{[1 + (z_0/f)^2]^{1/2}} \quad \text{and} \quad \mathrm{z}_0' = \frac{z_0}{1 + (z_0/f)^2}. \tag{9}$$

TABLE II
PARAMETERS OF EXCITATION LASERS CONSIDERED

Model	Spectra Physics Tsunami	Teem Photonics
Type	Ti:Sapphire femtosecond	Q-switched Nd:YAG
Lasing wavelength λ_{exc}	Tunable from 720 nm to 1050 nm	1065 nm
Pulse width Δt	100 fs	560 ps
Peak power P_p	145 kW	~18 kW
Energy per pulse E_p	~145 nJ	10.1 μJ
Pulse repetition frequency f_{rep}	80 MHz	6.9 kHz

For a Ti:sapphire laser tuned at 850 nm, the voxel dimensions are $W_{vx} = 8.08\,\mu$m and $L_{vx} = 3.50$ mm for a collimated beam at $\lambda_l = 977$ nm with a beam diameter $D_{\text{B}} = 4$ mm before being focused by a lens with a focal length $f = 150$ mm. In this case, and assuming that the laser beam is focused in the volumetric display from the bottom side of the display, the resolution along the vertical direction in a $35\text{ cm} \times 35\text{ cm} \times 35$ cm display would be 100 pixels. This resolution can be increased with the use of a more tightly focused beam.

The luminance in nits $(\text{cd} \cdot \text{m}^{-2})$ of the light emitted by a voxel, which is proportional to the optical power emitted per unit of area, can be calculated from (4) to (9) and from the Beer's law as

$$B = \kappa\sigma_{2p}\Phi C I_p^2 W_{vx}\Delta t f_{\text{rep}} \frac{\lambda_{\text{exc}}}{\lambda_{\text{emi}}} \exp(-\sigma_{a,\text{emi}} C L_{\text{view}}) \quad (10)$$

where λ_{emi} is the peak emission wavelength of the QDs, λ_{exc} is the wavelength of the excitation source, $I_p = P_p/(\pi W_0'^2)$ is the peak irradiance of the excitation source in the voxel, $\sigma_{a,\text{emi}} = 0.23\sigma_a$ is the effective absorption coefficient at the emission spectrum of the QDs (approximately 23% of the absorption coefficient at the first exciton peak), L_{view} is the optical path between the voxel and the observer inside the QD dispersion, and P_p and Δt are described in Table II. The parameter $\kappa = 683/16$ in (10) is a constant that is required to express the luminance in nits. The derivation of this expression is given in the Appendix.

The minimum concentration of QDs for a Q-switched Nd:YAG laser that satisfies the minimum luminance for normal display operation, $B \geq 100$ nit with $L_{\text{view}} = 17.5$ cm, was calculated from (10) at $C_{\min} = 2.36 \times 10^{14}$ cm^{-3}. This value was confirmed experimentally in Section III for an equivalent experimental setup. For a Ti:sapphire laser operating at $\lambda_{\text{exc}} = 977$ nm, the minimum concentration that satisfies the required minimum luminance was calculated at $C_{\min} = 1.037 \times 10^{12}$ cm^{-3}. Because of the higher peak power produced by the Ti:sapphire femtosecond laser, this value is two orders of magnitude lower than the minimum concentration required if a Q-switched Nd:YAG laser was used.

In these calculations we assumed that a single voxel is turned on with 100 nit of luminance. In the practical case of a volumetric image, for the power specified in the lasers, the minimum concentration $C_{\min}$ has to be increased proportionally to the number of voxels, which affects the effective value of f_{rep} in (10).

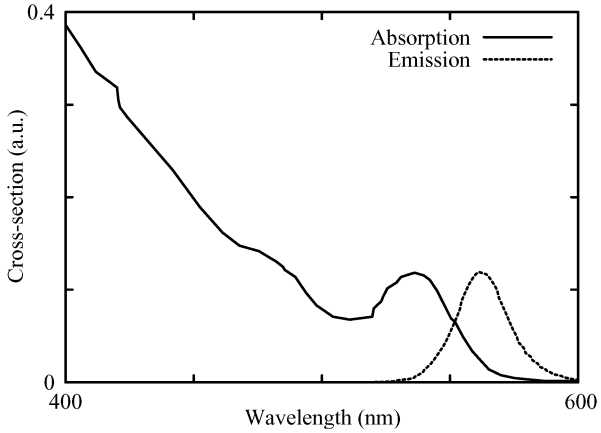

Fig. 1. Absorption and emission cross-section spectra (arbitrary units) of 560 nm core-shell CdSe/ZnS.

One important question to address is how realistic the calculated minimum concentration is. The concentration of the QDs in the dispersion can be calculated from the following equation:

$$C = N_A c \quad (11)$$

where C is the number concentration, QDs/cm^3; N_A is the Avogadro constant $\approx 6.022 \times 10^{23}$ mol^{-1}; c is the molar concentration, mol $\cdot$ cm^{-3}. A typical value for the molar concentration of 560 nm CdSe/ZnS QDs in 1 cm^3 is 54 nmol [46], which yields a concentration of 3.25×10^{16} QDs/cm^3. Therefore, approximately 0.073 mg of dry powder QDs will need to be dispersed in 1 cm^3 of the display medium to achieve the minimum concentration calculated from (10) if an Nd:YAG laser was used. The total quantity required for a 35/35/35 cm display would be 3.1 g. In this case, the coefficient of filling (the ratio of the actual concentration to the total saturation value) is only 0.73%. This number for the femtosecond laser would be much smaller, just 31.89 ppm.

III. EXPERIMENTAL DEMONSTRATION OF TECHNOLOGY

A series of TPA experiments were carried out to prove the technical feasibility of the proposed approach for creating a single voxel for a volumetric display using a *Teem Photonics* passively Q-switched 1064-nm Nd:YAG microchip laser with specifications given in the last column of Table II. The display medium was a dispersion of 10 mg 560 nm core-shell CdSe/ZnS QD in 1-ml toluene, procured from *Ocean Nanotech*. The absorption spectrum for this material with an emission peak of 560 nm and an absorption peak of 538 nm is shown in Fig. 1.

The experimental dispersions were placed in a 10-mm GL14-C quartz cuvette from *Starna Cell* with 10 mm pathlength size and two polished parallel optical windows. The starting material was additionally diluted with toluene to various concentrations. The molar concentration of the QDs in the dispersions was calculated from the Beer–Lambert law:

$$c = \frac{A}{\varepsilon\lambda} \quad (12)$$

TABLE III
ABSORBANCE, CONCENTRATION, VOXEL LUMINANCE AND SIZE

Absorbance	C (10^{14} cm^{-3})	Median Luminance (0-255)	Mean Diameter (mm)
0.108233	5.83	40	1.5
0.147603	7.97	59	1.8
0.182931	9.88	81	1.9
0.280827	15.16	120	1.9

where c is the molar concentration, M $\cdot$ cm^{-3}; A is the absorbance at the peak position of the first exciton absorption peak; ε is the molar extinction coefficient, L$\cdot$M$^{-1}\cdot$cm^{-1}; ℓ is the pathlength, cm. The molar extinction coefficient was assumed $= 1.115 \times 10^5$ L$\cdot$M$^{-1}\cdot$cm^{-1} following Yu *et al.* [47]. Once the molar concentration was calculated, the number concentration of QDs in the dispersion was determined from (11). The results for the measured absorbance and calculated concentrations are shown in Table III along with the measured median luminance and the mean diameter of the voxels generated in the dispersions. To carry out the absorbance measurements, we used an *Intelite* CW 532 nm frequency-doubled Nd:YAG laser with 5 mW of power.

The beam of the 1064 nm Q-switched laser was focused in the middle of the dispersion. To avoid the use of a beam expander, we used a lens with the focal length equal to 25 mm located at the beam waist of the laser, whose beam waist radius was equal to 250 μm. With these beam parameters, the estimated from (8) voxel dimensions were $W_{vx} = 11.6$ μm and $L_{vx} = 3.33$ mm, which are comparable to those obtained in Section II for a lens with a much longer focal length focusing a wider laser beam.

The first voxel was clearly visible with a naked eye at a concentration of 5.83×10^{14} cm^{-3}, an experimental value fairly close to the theoretical value of 3.88×10^{14} cm^{-3} predicted by (10) with $L_{\text{view}} = 0.5$ cm for a voxel with luminance $B = 100$ nit. With the concentration for the first visible voxel used in (10), the luminance was calculated at $B = 149$ nit. This difference between experiment and theory can be attributed to the imperfect optics that leads to a non-Gaussian profile of the beam at the voxel, and to the numerical deviation in the values used for the parameters in (10). There should be also a loss of light due to the reflection at the toluene–quartz interface and at the quartz-air interface.

Fig. 2 shows a typical result from the TPA experiments in which a well-defined voxel was successfully generated in the dispersion. Table III shows the values for the voxel luminance and diameter measured from the optical photographs for different concentrations. The voxel luminance was measured from the histogram in the green channel of the image. The luminance values represent the median of the histogram on a scale of 0 (dark) to 255 (light). These values are also plotted as a function of the QD concentrations in Fig. 3 showing the good agreement between the experimental and theoretical results.

IV. CONCLUSION

We demonstrated that individual voxels emitting visible light in all direction can be created through TPA in QDs dispersed in a transparent medium at the focal point of commercially available pulsed infrared lasers. We investigated this phenomenon theoretically through the derivation of a closed form expression for the luminance of a voxel generated in the material, which we experimentally validated. We are currently extending this study to multicolor volumetric displays based on two-photon absorption in QD dispersions, which will be based on a mixture of QDs, including blue- and red-emitting QDs. Because of the high photo-stability of the QDs, their large TPA cross-section, their impressive quantum efficiency, and the size dependence of the emission wavelength, QDs dispersed in a transparent host material hold a promise to become the preferred display material for practical volumetric displays. Such displays would have numerous military and civilian applications.

Fig. 2. Single green voxel generated by TPA in a 7.97×10^{14} cm^{-3} concentration of 560 nm core-shell CdSe/ZnS QD in toluene. Photograph taken with a 950–1070 OD7+ filter.

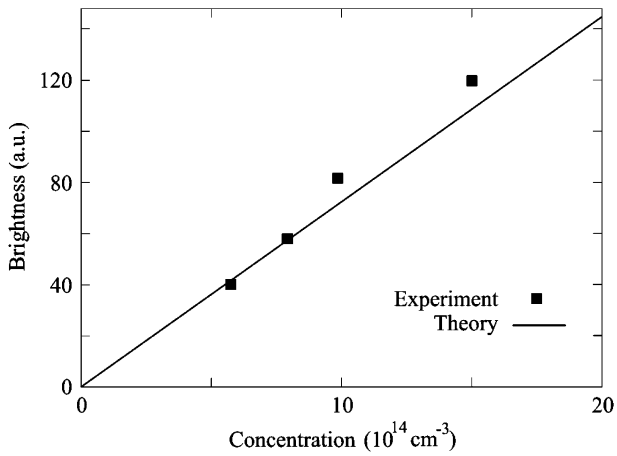

Fig. 3. Relative luminance of voxel as a function of the QD concentration in the dispersion. The dots are the experimental results. The solid line are results of (10) with the vertical axis rescaled by a factor of 0.4.

APPENDIX

In this appendix, we show the derivation of the expression (10) for the luminance of a voxel generated in QDs dispersed in a transparent solution and excited by a focused laser beam. The optical power emitted inside a voxel in all directions is proportional to the product between the quantum efficiency, Φ, and the absorbed power, which is equal to the irradiance multiplied by the transversal area of the voxel. The optical power emitted is also proportional to the ratio between the emitted photon energy and twice the photon energy of the excitation source. This last term accounts for the energy absorbed from the excitation laser that is lost due to vibrational relaxation in the QDs. The optical power emitted by the quantum dots in a voxel is equal to

$$P_{\text{emitted}} = \Phi \times \sigma_{2p} C I_p^2 L_{vx} \Delta t f_{\text{rep}} \times \pi W_{vx}^2 \times \frac{\lambda_{\text{exc}}}{2\lambda_{\text{emi}}}. \quad (13)$$

The parameters in (13) are given in Section II-C. The luminance of the voxel is proportional to the optical power emitted by the voxel divided by the voxel area projected along the viewing direction. Because the excitation source is most likely located at the bottom of the volumetric display and the viewing direction will be primarily from the sides of the display, the area of the voxel viewed from the viewing direction will be equal to the longitudinal area of the voxel. The longitudinal area of the voxel is equal to $A_{\text{long}} = 2W_{vx}L_{vx}$. Since the conversion factor from W/m^2 to 1 nit is $683/(4\pi)$, multiplying (13) by this factor and dividing the result by the longitudinal area A_{long} results in the expression for the luminance in nits shown in (10).

Since the light emitted by the voxel can be, depending on the concentration, significantly absorbed by the QD dispersion because of the overlap between the emission and the absorption spectrum, part of the light produced by the voxel will be reabsorbed in the QD dispersion and will not contribute to the luminance. Therefore, the expression that corrects the value of the voxel luminance, which follows the Beer's law because the voxel light is not directional and weak, is

$$B = B_o \exp(-\sigma_{a,\text{emi}} C L_{\text{view}}) \quad (14)$$

where B_0 would have been the value of the luminance in the absence of overlap between the emission and the absorption spectrum. The other parameters in (14) are described in Section II-C. The exponential term in (14) can not only lead to a reduction in the effective luminance, but can also give rise to a background glow due to the emission from the QDs that are not at the focal point. Therefore, (14) can be used as the guideline to determine the maximum QD concentration that can be used in the QD dispersion.

ACKNOWLEDGMENT

The authors would like to thank Dr. G. Gillispie of Fluorescence Innovations, Inc., Bozeman, MT, for valuable discussions about the project.

REFERENCES

[1] T. DeFanti, M. Brown, and B. McCormick, "Visualization: Expanding scientific and engineering research opportunities," *Computer*, vol. 8, pp. 12–16, 1989.

[2] D. D. Hearn and M. P. Baker, *Computer Graphics With OpenGL*, 3rd ed. Englewood Cliffs, NJ: Prentice Hall, 2003.

[3] E. Whitesell and R. Scheps, "Three dimensional volumetric display," U.S. Patent 6 466 184, Oct. 15, 2002.

[4] G. Favalora, "Volumetric 3D displays and application infrastructure," *Computer*, vol. 8, pp. 37–44, 2005.

[5] B. Blundell, A. Schwarz, and D. Horrell, "Volumetric three-dimensional display systems: Their past, present and future," *Eng. Sci. Edu. J.*, vol. 5, pp. 196–200, 1993.

[6] J. Geng, "Volumetric 3D display for radiation therapy planning," *J. Display Technol.*, vol. 4, no. 4, pp. 437–450, Dec. 2008.

[7] B. Javidi and S. Hong, "Three-dimensional holographic image sensing and integral imaging display," *J. Display Technol.*, vol. 2, no. 2, pp. 341–346, Dec. 2005.

[8] "Volumetric Display," [Online]. Available: http://www.wikipedia.com Access date: April 15, 2009

[9] E. Downing, "System and method using layered structure for three-dimensional display of information based on two-photon upconversion," U.S. Patent 5 956 172, Sep. 21, 1999.

[10] M. A. Bass, Rapaport, and H. Jennsen, "Dispersed crystallite up-conversion displays," U.S. Patent 6 654 161, Nov. 25, 2003.

[11] E. Downing, L. Hesselink, J. Ralston, and R. Macfarlane, "A three-color, solid-state, three-dimensional display," *Science*, vol. 273, pp. 1185–1189, 1996.

[12] M. Bass and H. Jennsen, "Display medium using emitting particles dispersed in a transparent host," U.S. Patent 6 501 590, Dec. 31, 2002.

[13] M. Bass, J. Eichenholz, and A. Rapaport, "Optically written display," U.S. Patent 6 897 999, May 24, 2005.

[14] A. Parker, "Mighty small dots," *Sci. & Technol. Rev.*, pp. 20–21, 2000.

[15] X. Sun and J. Liu, "System and method for a three-dimensional color image display utilizing laser induced fluorescence of nanopartcles and organometallic molecules in a transparent medium," U.S. Patent Appl. 2004/0227694.

[16] H. Kimura, T. Uchiyama, and H. Yoshikawa, "Laser produced 3D display in the air," in *Proc. ACM SIGGRAPH '06*, 2006, p. 20.

[17] Z. Q. Hao, J. Zhang, X. Lu, T. T. Xi, Y. T. Li, X. H. Yuan, Z. Y. Zheng, Z. H. Wang, W. J. Ling, and Z. Y. Wei, "Spatial evolution of multiple filaments in air induced by femtosecond laser pulses," *Opt. Express*, vol. 2, pp. 773–778, 2006.

[18] S. V. Gaponenko, *Optical Properties of Semiconductor Nanocrystals*. Cambridge, MA: Cambridge Univ. Press, 2003.

[19] A. Milnes and D. Feucht, *Heterojunctions and Metal-Semiconductor Junction*. New York: Academic, 1972.

[20] A. Alivisatos, "Semiconductor clusters, nanocrystals, and quantum dots," *Science*, vol. 271, pp. 933–937, 1996.

[21] M. Vasilevskiy, E. Anda, and S. Makler, "Electron-phonon interaction effects in semiconductor quantum dots: A nonperturabative approach," *Phys. Rev. B*, vol. 70, 2004, Art. id. 035318.

[22] L. E. Brus, "Electron-electron and electron-hole interactions in small semiconductor crystallites: The size dependence of the lowest excited electronic state," *J. Chem. Phys.*, vol. 80, pp. 4403–4410, 1984.

[23] A. Yoffe, "Semiconductor quantum dots and related systems: Electronic, optical, luminescence and related properties of low dimensional systems," *Adv. Phys.*, vol. 50, pp. 1–208, 2001.

[24] L. Banyai, P. Gilliot, Y. Z. Hu, and S. W. Koch, "Surface-polarization instabilities of electron-hole pairs in semiconductor quantum dots," *Phys. Rev. B*, vol. 45, pp. 14136–14142, 1992.

[25] B. O. Dabbousi, R. Rodriguez-Viejo, F. V. Mikulec, J. R. Heine, H. Mattoussi, R. Ober, K. F. Jensen, and M. G. Bawendi, "(CdSe) ZnS core-shell quantum dots: Synthesis and characterization of a size series of highly luminescent nanocrystallites," *J. Phys. Chem. B*, vol. 101, pp. 9463–9475, 1997.

[26] S. Weiss, M. C. Schlamp, and A. P. Alivisatos, "Electronic displays using optically pumped luminescent semiconductor nanocrystals," U.S. Patent 6 864 626, Mar. 8, 2005.

[27] M. J. Bowers, II, J. R. McBride, and S. J. Rosenthal, "White-light emission from magic-sized cadmium selenide nanocrystals," *J. Amer. Chem. Soc.*, vol. 44, pp. 15378–15379, 2005.

[28] D. R. Larson, W. R. Zipfel, R. M. Williams, S. W. Clark, M. P. Bruchez, F. W. Wise, and W. W. Webb, "Water-soluble quantum dots for multiphoton fluorescence imaging in vivo," *Science*, vol. 300, pp. 1434–1436, 2003.

[29] E. Poles, D. C. Selmarten, O. I. Micic, and A. J. Nozik, "Anti-stokes photoluminescence in colloidal semiconductor quantum dots," *Appl. Phys. Lett.*, vol. 75, pp. 971–973, 1999.

[30] Y. P. Rakovich, S. A. Filonovich, M. J. M. Gomes, J. F. Donegan, D. V. Talapin, A. L. Rogach, and A. Eychmuller, "Anti-stokes photoluminescence in II-VI colloidal nanocrystals," *Phys. Status Solidi. B.*, vol. 229, pp. 449–452, 2002.

[31] X. Wang, W. W. Yu, J. Zhang, J. Aldana, X. Peng, and M. Xiao, "Photoluminescence upconversion in colloidal CdTe quantum dots," *Phys. Rev. B*, vol. 68, 2003, id. 125318.
[32] K. I. Rusakov, A. A. Gladyshchuk, Y. P. Rakovich, J. F. Donegan, S. A. Filonovich, M. J. M. Gomes, D. V. Talapin, A. L. Rogach, and A. Eychmüller, "Control of efficiency of photon energy up-conversion in CdSe/ZnS quantum dots," *Opt. Spectroscopy*, vol. 94, pp. 859–863, 2003.
[33] W. Chen, A. G. Joly, and D. E. McCready, "Upconversion luminescence from CdSe nano-particles," *J. Chem. Phys.*, vol. 122, 2005, id. 224708.
[34] P. P. Paskov, P. O. Holtz, B. Monemar, J. M. Garcia, W. V. Schoenfeld, and P. M. Petroff, "Photoluminescence up-conversion in InAs/GaAs self-assembled quantum dots," *Appl. Phys. Lett.*, vol. 77, pp. 812–814, 2000.
[35] A. M. van Oijen, R. Verberk, Y. Durand, J. Schmidt, J. N. J. van Lingen, A. A. Bol, and A. Meijerink, "Continuous-wave two-photon excitation of individual CdS nano-crystallites," *Appl. Phys. Lett.*, vol. 79, pp. 830–832, 2001.
[36] M. Y. Valakh, N. O. Korsunska, Y. G. Sadofyev, V. V. Strelchuk, G. N. Semenova, L. V. Borkovska, V. V. Artamonov, and M. V. Vuychik, "Anti-stokes photoluminescence and structural defects in CdSe/ZnSe nanostructures," *Mat. Sci. Eng. B*, vol. 101, pp. 255–258, 2003.
[37] A. G. Joly, W. Chen, D. E. McCready, J. O. Malm, and J. O. Bovin, "Upconversion luminescence of CdTe nanoparticles," *Phys. Rev. B*, vol. 71, 2005, id. 165304.
[38] S. C. Pu, M. J. Yang, C. C. Hsu, C. W. Lai, C. C. Hsieh, S. H. Lin, Y. M. Cheng, and P. T. Chou, "The empirical correlation between size and two-photon absorption cross section of CdSe and CdTe quantum dots," *Small*, vol. 2, pp. 1308–1313, 2006.
[39] N. Thantu, "Second harmonic generation and two-photon luminescence upconversion in glasses doped with ZnSe nanocrystalline quantum dots," *J. Luminesc.*, vol. 111, pp. 17–24, 2005.
[40] M. Jacobsohn and U. Banin, "Size dependence of second harmonic generation in CdSe nanocrystal quantum dots," *J. Phys. Chem. B*, vol. 104, pp. 1–5, 2000.
[41] J. W. M. Chon, M. Gu, C. Bullen, and P. Mulvaney, "Three-photon excited band edge and trap emission of CdS semiconductor nanocrystals," *Appl. Phys. Lett.*, vol. 84, pp. 4472–4474, 2004.
[42] W. Z. Wu, Z. R. Zheng, W. L. Liu, J. P. Zhang, Y. X. Yan, Q. H. Jin, Y. Q. Yang, and W. H. Su, "Upconversion luminescence of CdTe nanocrystals by use of near-infrared femtosecond laser excitation," *Opt. Lett.*, vol. 32, pp. 1174–1176, 2007.
[43] C. R. Nave, Georgia State University, "HyperPhysics Concepts," [Online]. Available: http://hyperphysics.phy-astr.gsu.edu/hbase/hph.html Access date: April 24, 2009
[44] J. Fisher, B. Salzberg, and A. Yodh, "Near infrared two-photon excitation cross-sections of voltage-sensitive dyes," *J. Neurosci. Methods*, vol. 148, pp. 94–102, 2005.
[45] B. Saleh and M. Teich, *Fundamentals of Photonics*. New York: Wiley, 1991.
[46] Evident Technology, Quantum Dot Research Materials [Online]. Available: http://www.evidenttech.com Access date: April, 24, 2009
[47] W. W. Yu, L. Qu, W. Guo, and X. Peng, "Experimental determination of the extinction coefficient of CdTe, CdSe, and CdS nanocrystals," *Chem. Mater.*, vol. 15, pp. 2854–2860, 2003.

Ivan T. Lima, Jr. (S'96–M'03–SM'09) was born in Juazeiro, State of Bahia, Brazil. He received the B.Sc. degree in electrical engineering from the Federal University of Bahia (UFBA), Salvador, Brazil, in 1995, the M.Sc. degree in electrical engineering from the State University of Campinas (UNICAMP), Campinas, Brazil, in 1998, and the Ph.D. degree in electrical engineering in the field of photonics from the University of Maryland, Baltimore County (UMBC), Baltimore, in 2003.

From 1986 to 1996, he was with the Banco do Brasil (Bank of Brazil), where he served as an Information Technology Adviser of the State Superintendence of Bahia, Brazil. From 1998 to 2003, he was a Research Assistant in the Optical Fiber Photonics Laboratory at the UMBC. In 2003, he became an Assistant Professor in the Department of Electrical and Computer Engineering, North Dakota State University (NDSU), Fargo. From July 2007 to October 2008, he also served at the Center for Nanoscale Science and Engineering (CNSE), NDSU, as a Faculty Associate. In 2006, he served as Faculty Fellow in the 2006 Air Force Summer Faculty Fellowship Program in the Wright-Patterson Air Force Research Laboratory in Dayton, OH. Since October 2008, he is holding the Visiting Professor status in the Department of Electrical and Computer Engineering, University of Manitoba, Winnipeg, MB, Canada. He has authored and coauthored 25 archival journal papers, 52 conference contributions (14 invited), one book chapter, one U.S. Patent, and one provisional U.S. Patent.

Dr. Lima received the IEEE LEOS Graduate Student Fellowship Award in 2003, and he was a co-recipient of the Venice Summer School on Polarization Mode Dispersion Award. In 2009 he was elevated to the grade of Senior Member of the IEEE. From 2004 to 2009, he served as co-instructor (invited) of the Short Course SC210: Hands-on Polarization Measurement Workshop at the Optical Fiber Communications Conference and Exposition (OFC): Anaheim (2003, 2005, 2006, and 2007), Los Angeles (2004), and San Diego (2008, 2009). From 2007 to 2011, he is serving as the project director of the U.S.-Brazil Engineering Education Consortium on Renewable Energy that is funded by the U.S. Department of Education.

Val R. Marinov was born in Plovdiv, Bulgaria. He graduated magna cum laude with B.Sc. and M.Sc. degrees in manufacturing engineering from the Technical University, Rousse, Bulgaria, in 1979. He received his Ph.D. degree in manufacturing engineering from the Technical University of Sofia, Bulgaria in 1992.

He has seven years of industrial and more than 22 years of academic experience in the area of manufacturing engineering for metal, plastic, and electronic products. Currently, he is an Associate Professor of Manufacturing Engineering at North Dakota State University (NDSU), Fargo, ND. Prior to joining NDSU in January 2001, he served on the faculty at Eastern Mediterranean University, Cyprus (1997–2000). His prior affiliations include the Department of Manufacturing Engineering at the Technical University in Plovdiv, Bulgaria (1987–1997), and the Laboratory for Precision Machining and Machine Tools, Korea Advanced Institute of Science and Technology, Taejon, South Korea (1993–1994). Since 2002 he has been associated with the NDSU Center for Nanoscale Science and Engineering (CNSE) where he is a research team leader managing numerous research projects in the area of advanced packaging methods for flexible microelectronics systems, including using lasers for packaging bare dies.

Dr. Marinov has coauthored a book on modeling and simulation of the material removal process in 1997, and more recently, a chapter on laser sintering of direct-write nanosized materials. He has (co)authored over thirty publications in broad and diversified areas, including theory of material removal, finite-element modeling, tribology, direct-write methods for microelectronics packaging, and most recently, high-density interconnect technology for flexible electronics.